An Extended Non-local Means Algorithm: Application to Brain MRI

Muhammad Aksam Iftikhar,[1,2] Abdul Jalil,[1] Saima Rathore,[1,3] Ahmad Ali,[1] Mutawarra Hussain[1]

[1] Department of Computer and Information Sciences, Pakistan Institute of Engineering and Applied Sciences, Nilore, Islamabad, Pakistan

[2] Department of Computer Science, COMSAT institute of information technology, Lahore, Pakistan

[3] Department of Computer Science and Information Technology, University of Azad Jammu and Kashmir, Muzaffarabad, Azad Kashmir

Received 23 April 2014; revised 14 June 2014; accepted 5 August 2014

ABSTRACT: Improved adaptive nonlocal means (IANLM) is a variant of classical nonlocal means (NLM) denoising method based on adaptation of its search window size. In this article, an extended nonlocal means (XNLM) algorithm is proposed by adapting IANLM to Rician noise in images obtained by magnetic resonance (MR) imaging modality. Moreover, for improved denoising, a wavelet coefficient mixing procedure is used in XNLM to mix wavelet subbands of two IANLM-filtered images, which are obtained using different parameters of IANLM. Finally, XNLM includes a novel parameter-free pixel preselection procedure for improving computational efficiency of the algorithm. The proposed algorithm is validated on T1-weighted, T2-weighted and Proton Density (PD) weighted simulated brain MR images (MRI) at several noise levels. Optimal values of different parameters of XNLM are obtained for each type of MRI sequence, and different variants are investigated to reveal the benefits of different extensions presented in this work. The proposed XNLM algorithm outperforms several contemporary denoising algorithms on all the tested MRI sequences, and preserves important pathological information more effectively. Quantitative and visual results show that XNLM outperforms several existing denoising techniques, preserves important pathological information more effectively, and is computationally-efficient. Int J Imaging Syst Technol, 24, 293–305, 2014; Published online in Wiley Online Library (wileyonlinelibrary.com). DOI: 10.1002/ima.22106

Key words: nonlocal means; denoising; brain MRI; Rician noise; wavelet

Correspondence to: Muhammad Aksam Iftikhar;
e-mail: aksam.iftikhar@gmail.com

Grant sponsors: This research work is supported by PIEAS-administered Endowment Fund, provided by Higher Education Commission Pakistan, for higher education and R&D in IT and Telecom Sectors.

I. INTRODUCTION

Magnetic resonance imaging (MRI) is a popular noninvasive and in vivo nuclear imaging technique, which exposes important biological structures in the scanned body part. Radiologists infer important pathological information from the analysis of magnetic resonance (MR) images of the examined organ. This analysis is automated in computer-aided diagnosis (CAD) systems to provide a secondary opinion to the radiologists for taking more confident and reliable decisions. Moreover, a CAD system expedites the process of diagnosis by processing many images simultaneously. However, a CAD system analyzing MRI may produce incorrect results, as these images inevitably suffer from thermal noise due to the tradeoff between their acquisition time and signal to noise ratio. The acquisition time is practically limited due to physical limitations and patient comfort. Therefore, the noise should be explicitly removed from these images using post processing denoising techniques.

Denoising of MRIs imposes special requirements on the denoising process, since the preservation of features of interest is more important than merely generating an image which is visually more pleasing. Undesirable artifacts introduced in MRIs during the denoising process may be mistreated as clinically important features. Therefore, robust methods for MRI denoising are in high demand. These methods should also explicitly consider the special nature of noise in MRIs during the denoising process. The noise in magnitude MRIs follows Rician distribution, which introduces certain bias into these images. This bias differently affects various regions in images with different intensity distribution. The denoising method should explicitly remove this bias of Rician noise to yield optimal performance. For these reasons, brain MRI denoising is an active area of research these days.

The traditional approaches to image denoising include wavelet filtering (Donoho 1995; Selesnick 2004; Luisier et al., 2007; Wen et al., 2013), total variation minimization (Osher et al., 2005;

Gupta et al., 2013), diffusion filtering (Perona and Malik, 1990; Gilboa et al., 2004), and local neighborhood based filtering (Tomasi and Manduchi, 1998). Nonlocal means (NLM) (Buades et al., 2005) is a relatively recent denoising method, which has been applied to brain MRI denoising (Coupe et al., 2008; Manjon et al., 2008). It removes noise from an image while preserving sufficient image details. The intensity value of a pixel is restored by computing weighted sum of pixels within a search window around the pixel. The weights are computed based on Euclidean distance between intensity values of patches (local neighborhoods) of pixels. Aksam et al. (2012) applied NLM for brain MRI denoising, and obtained optimal values of its parameters with the help of a variant of genetic algorithm. Further, they proposed a variant of classical NLM, namely improved adaptive nonlocal means (IANLM) algorithm, and applied it for brain MRI denoising (Iftikhar et al., 2013). The IANLM algorithm makes the search window size adaptive with the help of a search window adaptation mechanism, and a robust threshold criterion. An alternate spiral window traversal mechanism is also implemented in IANLM, which improves its robustness due to the characteristic of image smoothness. Iftikhar et al. (2014) proposed an enhanced nonlocal means (ENLM) algorithm, which adapts the IANLM algorithm to Rician noise using a bias correction method (Nicolas et al., 2008). The ENLM algorithm was validated using T1-weighted and T2-weighted brain MRI data.

Manjon et al. (2008) introduced an unbiased nonlocal means (UNLM) filter, which removes the bias introduced by Rician noise in MRIs. It filters the square magnitude MRI instead of the original image, and subtracts the bias value from intensity value of each pixel in the restored image. Coupe et al. (2008) proposed an optimized block-wise NLMs filter for denoising 3D brain MRIs. In the optimized NLMs filter, they presented a 3D implementation of NLM, and proposed automatic parameter tuning of the filter parameters. They also adapted the filter to Rician noise in a way similar to UNLM, and presented a voxel preselection procedure to select suitable set of pixels for computing weighted sum in the denoising process. However, the voxel preselection procedure presented therein requires additional parameters, which should be assigned appropriate values for a particular application. Vega et al. (2012) proposed an alternate approach to computation of similarity weights in the NLM algorithm, and validated their proposed algorithm on 3D brain MRI data. They suggested computing the distance between features of patches instead of intensity values of pixels in patches to compute the similarity weights. In addition to improving the quality of the filtered image, this approach had the inherent computational advantage, since the number of features are usually less in number than number of pixels in patches.

A wavelet sub-band mixing procedure has been proposed in (Szilagyi et al., 2003) for 3D brain MRI denoising, which combines different wavelet sub-bands of over- and under-smoothed images obtained using NLM filter. Combining different sub-bands in the wavelet domain exploits information in the low and high frequency components of images, thereby resulting in better-quality filtered image. The over- and under-smoothed images are obtained using different size of patch for each image, while keeping all other parameters of NLM the same in both images. Manjon et al. (2010) further exploited the concept of wavelets sub-band mixing method for dealing with spatially varying noise in MRIs. They made the proposed filter adaptive to spatially varying noise by incorporating information about local noise in the image.

Some of other state of the art denoising methods, different from nonlocal methodology, include patch-based locally optimal Wiener filtering (PLOW) (Chatterjee and Milanfar, 2012), block matching and 3D filtering (BM3D) (Dabov et al., 2007) and orthogonal wavelet transform based on SURE-LET principle (OWT-SURELET) (Luisier et al., 2007). The PLOW filter, contrary to NLM, exploits redundancy in both geometrically and photometrically similar patches. Photometric similarity is measured in a way similar to the NLM method, whereas the geometrically similar patches are identified by geometric clustering of image based on local image features. The BM3D filter groups similar 2D image blocks into 3D data arrays, and performs a collaborative filtering procedure on these data arrays to obtain jointly filtered grouped image blocks. These blocks are then aggregated to obtain the filtered image in which the fine details shared by grouped blocks are revealed. Finally, OWT-SURELET is a wavelet-domain method which strives to minimize the error between the noise-free and restored images in the mean square sense. The noise-free image is estimated from noisy image based on Stein's unbiased risk estimate.

In this work, we have extended our work on IANLM (an adaptive variant of classical NLM algorithm), and presented an extended nonlocal means (XNLM) algorithm. As mentioned previously, IANLM was adapted to Rician noise in ENLM using a bias correction method. In XNLM, the IANLM filter has been adapted to Rician noise using an alternate bias correction method, which results in improved denoising performance (Manjon et al., 2008). Moreover, a wavelet coefficients mixing (WCM) procedure has been used in XNLM to improve the quality of the restored images. The WCM procedure exploits valuable information from different wavelet subbands of the over- and under-smoothed images, which are obtained by IANLM filtering using different filter parameters (Coupe et al., 2008). Further, an automatic parameter-free pixel preselection process has been proposed to overcome the computational overhead incurred due to computation of two filtered images in WCM. The proposed pixel preselection method is simple to implement, and automatically adapts to the amount of noise in the input image. It considerably improves the computational efficiency of XNLM. Finally, optimal values of several parameters of XNLM have been obtained for application to brain MRI. Different variants of the proposed XNLM algorithm have been validated on simulated T1-, T2-, and PD-weighted brain MRIs. These variants test the influence of various extensions to standard IANLM algorithm, which are proposed in this work. Experimental results reveal that the proposed algorithm is more robust to noise, and preserves the integrity of pathological structures in the restored images.

The rest of the article is organized as follows. Section II describes in detail each component of the proposed technique and the data set used for validating the proposed technique. Detailed results of various denoising experiments and relevant discussion are presented in Section III. Finally, the research is concluded in Section IV.

II. MATERIALS AND METHODS

A. The Proposed Extended Nonlocal Means Algorithm. The proposed XNLM algorithm comprises various components, which are listed as follows:

1. IANLM filtering (Section II.A.1).
2. Pixel preselection (Section II.A.2).
3. Adaptation to Ricain noise (Section II.A.3).
4. Wavelets coefficient mixing (WCM) (Section II.A.4).
5. Optimization of different parameters of the algorithm (Section II.A.5).

These components should be applied to an input image to obtain the XNLM-filtered image. Figure 1 shows the XNLM process

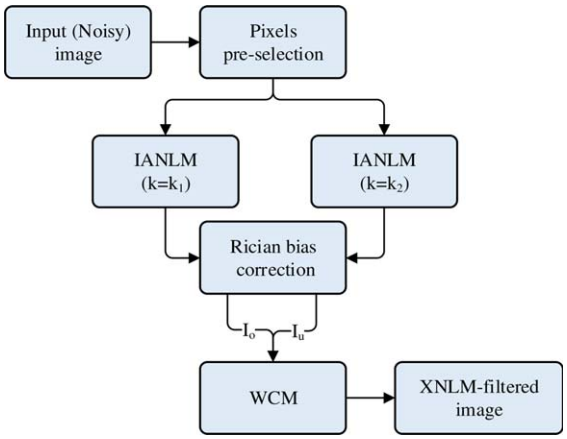

Figure 1. Block diagram of the proposed XNLM algorithm. [Color figure can be viewed in the online issue, which is available at wileyonlinelibrary.com.]

graphically in a flow chart. It should be noted that the pixel preselection is implemented as an inherent part of IANLM. However, it has been shown as a separate step in Figure 1 for better demonstration. In the next steps, the two IANLM-filtered versions of the input image are obtained using different values of the scaling parameter "k" (see Section II.A.5 for discussion on the parameter "k" and Section III.A for values of "k" used in this work), and adapted to Rician noise. Finally, the WCM procedure, described in Section II.A.4, is applied on the two images I_o and I_u to obtain the XNLM-filtered image. All the said components of XNLM are described in detail in the following text.

A.1 Improved Adaptive Nonlocal Means Algorithm. IANLM is a variant of classical NLM method based on dynamic adaptation of its search window size. In classical NLM, the search window is traversed exhaustively to compute the similarity of different patches in the window with the central patch. The similarity between pixel i and j is measured by weight w_{ij}. The denoising process in NLM is based on weighted sum of pixel intensity values within the search window. This is expressed mathematically as follows.

$$x_i = \sum_{j \in S_i} w_{ij} y_j, \quad \text{subject to} \quad \sum_{j \in S_i} w_{ij} = 1 \tag{1}$$

where y_j represents the jth pixel in the set of pixels (S_i) within the search window of pixel i, and x_i represents the NLM-restored value of pixel i. The term w_{ij} is the similarity weight between patches P_i (patch of pixel i is referred as P_i in the following text) and P_j, and is computed using the following expression:

$$w_{ij} = \frac{1}{Z_i} e^{-\frac{\left(\|y(P_i) - y(P_j)\|_2^2\right)}{h^2}} \tag{2}$$

where h is the smoothing factor, which controls the tradeoff between smoothness (noise removal) and detail preservation. The term $||y(P_i) - y(P_j)||^2$ denotes the Euclidian distance between patches P_i and P_j, where $y(P_i)$ and $y(P_j)$ are the intensity values of pixels in patches P_i and P_j, respectively. The term Z_i is a normalization constant, which makes sure that $w_{ij} \in [0, 1]$.

The exhaustive search process within the search window poses severe computational burden without much performance advantage. The IANLM algorithm presents an adaptation mechanism to automatically select the search window size for each pixel. The adaptation mechanism is based on number of fit pixels/patches found within particular search window. A fit pixel implies a pixel for which the similarity weight is superior to a predefined threshold. Thus, mathematical formulation of IANLM is given as follows.

$$x_i' = \sum_{j \in N_i^*} w_{ij} y_j, \quad \text{subject to} \quad \sum_{j \in N_i^*} w_{ij} = 1 \tag{3}$$

where x_i' is the restored value of pixel i using IANLM, and $N_i^* \subseteq S_i$ is the set of pixels around pixel i, satisfying the following constraints.

1. **Robust threshold criterion**: $w_{ij} > w_\theta$, where w_θ is the threshold on similarity between pixels i and j.
2. **Window adaptation test**: $|N_i^*| \leq N_f$, where N_f designates number of fit pixels within the search window.

An alternate implementation of the IANLM algorithm was also proposed in (Iftikhar et al., 2013). Traditionally, the search window is traversed in a row/column wise manner such that the pixel on top-left of the window is processed first. This traversal mechanism is replaced by a spiral traversal in IANLM, such that the central pixel is processed first and the search is progressed outward in a region growing manner. The alternate search traversal mechanism improves the denoising process due to the inherent smoothness generally present in local patches of an image (Iftikhar et al., 2013).

A.2 Pixel Preselection. The window adaptation mechanism proposed in IANLM algorithm not only reduces the computational burden but also improves denoising performance by considering only the suitable pixels within the search window. However, another computationally expensive task in the nonlocal denoising is the computation of similarity weighs. The computational burden can be further reduced by selecting pixels prior to computing actual weights. This pixel preselection process is also expected to improve the quality of the restored image by eliminating the irrelevant pixels, which might deteriorate the performance of IANLM.

In this article, we have proposed a pixel preselection process, which is simple to implement and requires no additional parameters. Further, it is adaptable to the amount of noise in the image. The proposed pixel preselection process is expressed as follows.

$$w_{ij} = \begin{cases} \dfrac{1}{Z_i} e^{-\frac{\left(\|y(P_i) - y(P_j)\|_2^2\right)}{h^2}}, & \text{if } |\overline{y_i} - \overline{y_j}| < \sigma \\ 0, & \text{otherwise.} \end{cases} \tag{4}$$

where $\overline{y_i}$ and $\overline{y_j}$ correspond to ith and jth pixel of the mean-filtered input image. The symbol $|.|$ represents the absolute operator, and σ is the standard deviation of noise in the input image. Thus, the proposed preselection process specifies that the similarity weight between pixel i and j should be computed according to Eq. (2), if the absolute difference of the corresponding pixels' values in the mean-filtered image is less than the standard deviation of noise in the image. Otherwise, the similarity weight between pixels i and j is simply set to 0. The intuition behind this criterion is that if the absolute difference is greater than σ, then the patches of pixels i and j are actually dissimilar and should be excluded from the denoising process. The term σ is set as threshold to tolerate the effect of noise in difference computation and adjust the preselection process according to amount of noise in the image. Thus, the proposed preselection procedure is free of any additional parameters and is adaptive to the amount of noise in the image.

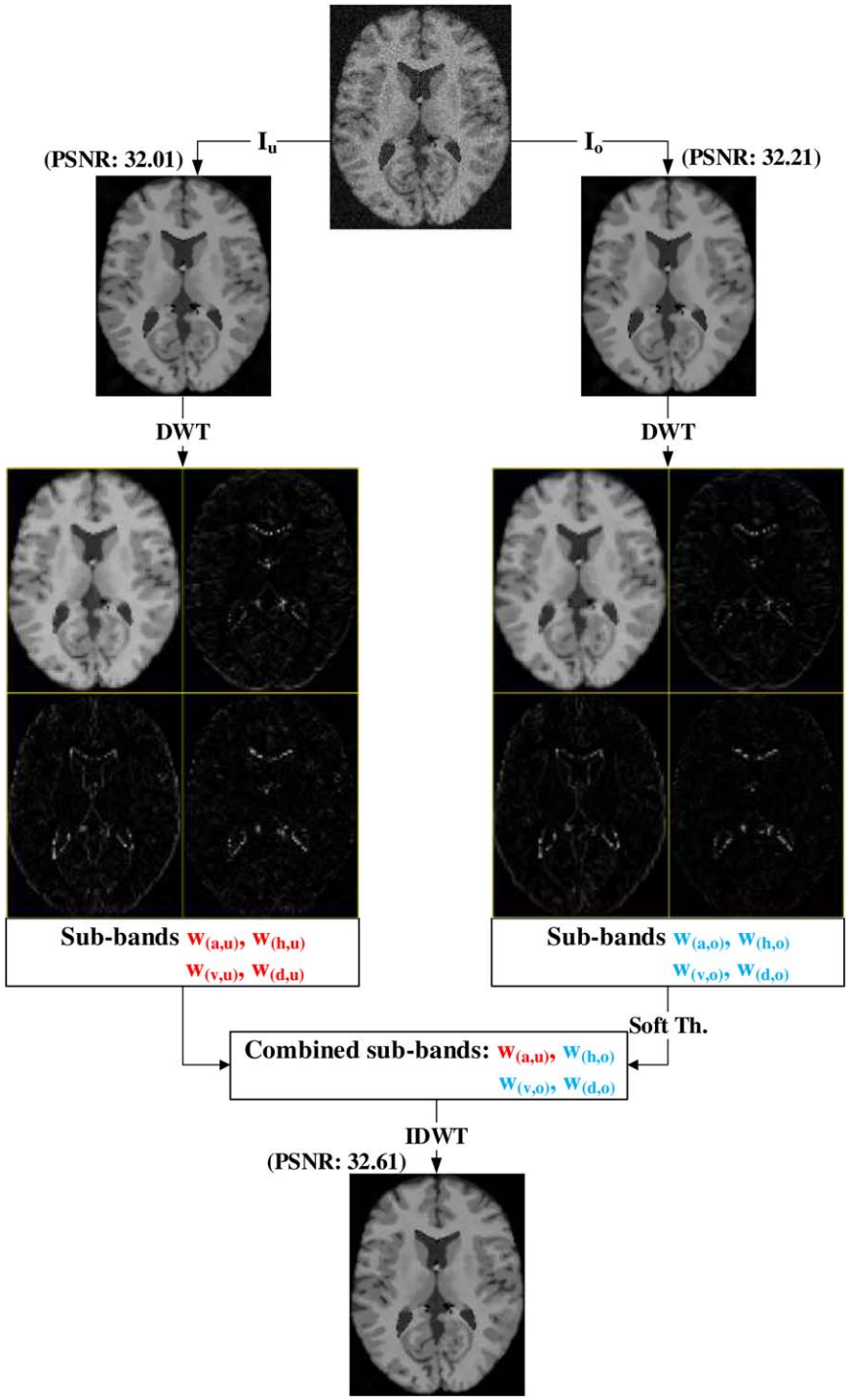

Figure 2. The proposed WCM procedure. [Color figure can be viewed in the online issue, which is available at wileyonlinelibrary.com.]

A.3 Adaptation to Rician Noise. MRIs usually contain Rician noise, which is known to be signal dependent. Rician noise exhibits different behavior in low and high intensity regions, thereby introducing bias and reducing overall contrast of an image. The value of Rician bias is generally equal to double the variance of the noise present in an image (Nowak, 1999). As stated earlier in Section I, the ENLM algorithm adapts IANLM to Rician bias using a bias correction method (Nicolas et al., 2008). In this work, we have adapted IANLM to Rician noise by applying an alternate bias correction method (Manjon et al., 2008), which is formulated as follows.

$$x_i'' = \sqrt{(\mathrm{IANLM}(y_i))^2 - 2\sigma^2} \tag{5}$$

where, y_i represents the value of ith noisy pixel, IANLM(y_i) represents the ith pixel value restored by IANLM, the term σ^2 is the variance of noise in the image, and x_i'' is the restored value after

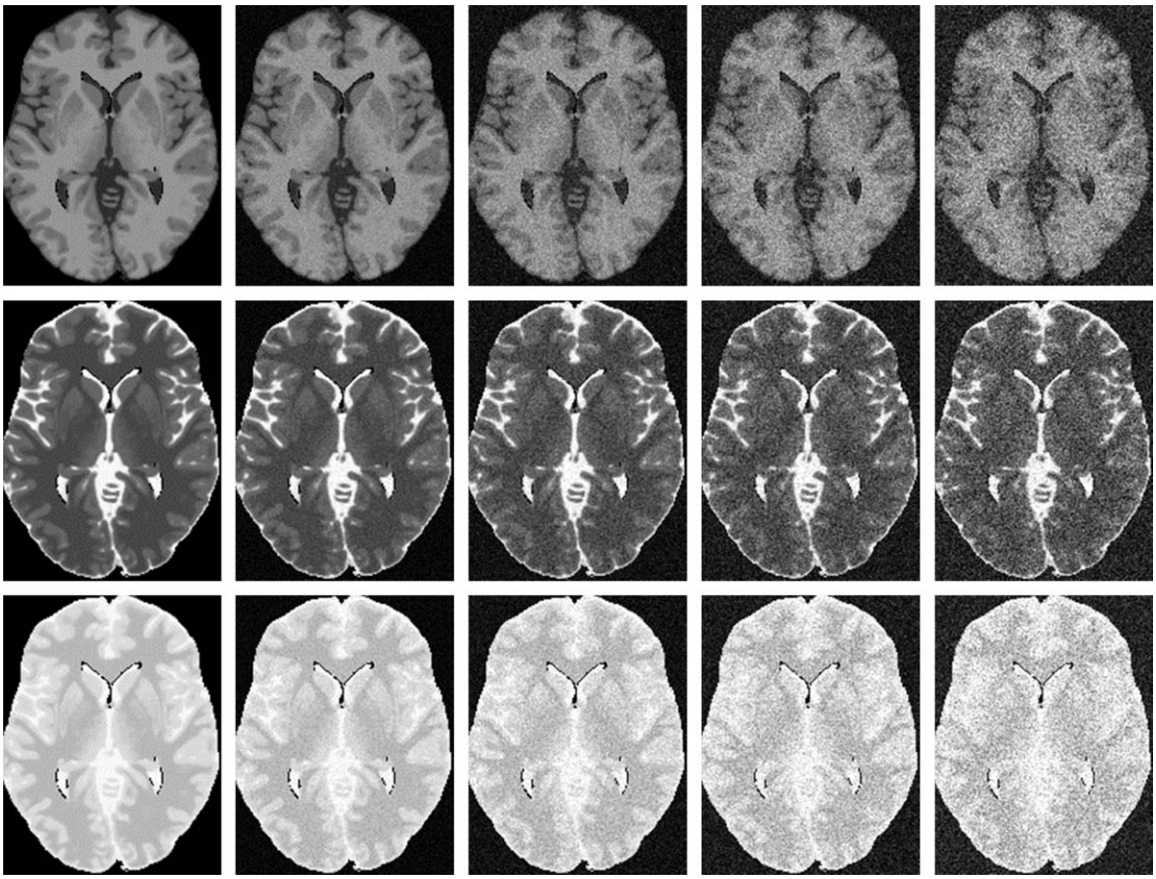

Figure 3. Brain MR images in different modalities with increasing level of noise. 1st row: T1-weighted images, 2nd row: T2-weighted images, and 3rd row: PD-weighted images. 1st column: noise-free images, 2nd–5th columns: noisy images with $\sigma = 7.5$, 15, 22.5, and 30, respectively.

applying the bias correction. The bias correction method implies that the bias value is subtracted from square of the restored value of each pixel. Experimental results reveal that the alternate bias correction method results in improved denoising performance (see Section III.B).

A.4 Wavelet Coefficients Mixing. Wavelet transforms an image into a different domain, wherein low and high frequency components of the image are separated into different sub-bands. The conventional approach in image denoising using wavelet filtering is to suppress such coefficients in different sub-bands which potentially correspond to image noise (Donoho, 1995; Öktem et al., 2002). These coefficients are determined by either hard thresholding or soft thresholding. In the hard thresholding method, the coefficients below a certain threshold are eliminated altogether. Conversely, the soft thresholding method suppresses the coefficients depending of their distance from the threshold. It can be formulated as follows.

$$c_{\text{soft}} = \begin{cases} \text{sgn}(c)(|c-\lambda|), & \text{if } c > \lambda \\ 0, & \text{if } c < \lambda \end{cases} \tag{6}$$

where c and c_{soft} represent the value of wavelet coefficient before and after applying the soft thresholding method, and λ is the threshold on coefficients, which can be computed using several methods existing in literature for the purpose (Chang et al., 2000; Fodor and Kamath, 2003). In general, soft thresholding yields better performance than hard thresholding.

In this article, we have used a procedure for mixing wavelet coefficients in the wavelet domain for better denoising. The WCM procedure exploits the capability of wavelets to segregate high and low frequency components of an image. In WCM, two versions of the filtered images, namely over-smoothed (I_{o}) and under-smoothed (I_{u}) images, are obtained using different parameters of IANLM. As the name implies, noise is removed effectively in the over-smoothed image, but fine structural details may be lost. On the contrary, image details are preserved in the under-smoothed image, but some noisy artifacts may still be present. The idea is to mix the coefficients of low and high frequency components of these images in the wavelet domain to exploit valuable information in both types of frequency components.

Wavelet transforms an image into approximation (a), and horizontal (h), vertical (v), and diagonal (d) detail sub-bands at level 1 in the new domain. Let, the wavelet sub-bands corresponding to I_{o} and I_{u} be denoted by $w_{(\text{x,o})}$ and $w_{(\text{x,u})}$, respectively, where $x \in [a, h, v, d]$ corresponds to the four sub-bands. The next step in the WCM procedure is to apply the soft thresholding method using minimax threshold (Donoho and Johnstone, 1998) on the coefficients in the detail sub-bands of I_{o}, that is, $w_{(\text{h,o})}$,$w_{(\text{v,o})}$,and $w_{(\text{d,o})}$. Then, the approximation sub-band $w_{(\text{a,u})}$ of I_{u} is combined with the detail sub-bands of I_{o}, and the image is transformed back into spatial domain. Due to the combination of sub-bands from the two preliminary filtered images,

Table I. Optimized values of parameters in different denoising algorithms.

	Parameters						
Noise (σ)	s	p	k	N_f	w_θ	w'	Wavelet
$XNLM_0/XNLM_1$	5	2 (T1),1(T2/PD)	1	60	0.01	0.1	–
$XNLM_2/XNLM$	5	2 (T1),1(T2 /PD)	1 (I_o), 0.9 (I_u)	60	0.01	0.1	sym8

the detail preservation and noise removal characteristics are retained in the final image.

Figure 2 graphically illustrates the mixing of wavelet coefficients for a T1-weighted brain MRI. Here, I_o and I_u have been decomposed into four wavelet sub-bands each using the discrete wavelet transform at first level. After soft thresholding and combining different sub-bands, inverse discrete wavelet transform is applied to obtain the final image. As shown in Figure 2, the quality of the final image, quantitatively measured by peak signal to noise ratio (PSNR) is better than both preliminary filtered images, that is, I_o and I_u.

A.5 Optimal Selection of Parameters. The proposed XNLM algorithm depends on a few parameters, which should be assigned suitable values for optimal denoising performance. The algorithm may suffer if one or more of these parameters are not assigned appropriate values for a particular application. The optimal selection of these parameters has been discussed in detail in the experimental section (see Section III.A).The following text briefly describes these parameters.

Search window size (s) The radius of a squared search window around a pixel of interest. A value of $s = 5$ implies that the dimensions of the search window are $(2s+1 \times 2s+1) = 11 \times 11$.

Patch size (p) The radius of a squared local neighborhood (patch) to be used for computation of similarity weights. A value of $p = 2$ means the dimensions of the patch are $(2p+1 \times 2p+1) = 5 \times 5$.

Scaling factor (k) The smoothing parameter (h) in Eq. (2) is related to the amount of noise in the image according to the equation $h = k\sigma$, where σ represents the amount (standard deviation) of noise, and k is the scaling factor (Manjon et al., 2008). The standard deviation of noise can be measured from the input image. Thus, it is the scaling factor that determines the value of smoothing parameter. Therefore, it must be assigned an appropriate value for a particular application.

Weight of central pixel (w') During the process of computing similarity weights, the weight of the central pixel always evaluates to 1, since both of the patches to be compared are the same. Hence, the restored value of current pixel is strongly biased toward the original noisy value. Therefore, the central pixel should be considered a special case, and should be assigned an appropriate value for optimal denoising performance.

Weight threshold (w_θ) This parameter is exclusively included in IANLM, and is not part of the traditional NLM algorithm. This parameter represents a threshold on similarity weights, which is applied to determine the set of pixels participating in the denoising process (see Section II.A.1).

Desired number of fit patches (N_f) Similar to w_θ, this parameter is also exclusive to IANLM. Its value determines the number of fit pixels to be searched in a window before the search is trancated (see Section II.A.1).

B. Proposed Variants of XNLM. In this work, following variants of the proposed XNLM algorithm have been presented for individually investigating the influence of different extensions proposed in XNLM on denoising performance.

- $XNLM_0$ (Nonspiral IANML + bias correction) implements IANLM using conventional row/column wise window traversal. Moreover, IANLM is adapted to Rician noise as described in Section II.A.3. The influence of Rician bias correction on denoising performance can be realized using this variant.
- $XNLM_1$ (Spiral IANLM + bias correction) is similar to $XNLM_0$ except that it implements IANLM with spiral window traversal as proposed in (Iftikhar et al., 2013).This variant, when comapred to $XNLM_0$, facilitates the realization of the performance advantage of sprial implementation over conventional row/column wise traversal.
- $XNLM_2$ (Spiral IANLM + bias correction + WCM) also implements the WCM procedure in $XNLM_1$. The improvement induced due to WCM can be realized using this variant.
- XNLM (Spiral IANLM + bias correction + WCM + pixel preselection) includes all the extensions incorporated to IANLM in this research work.

C. Data Set. The proposed algorithm has been validated on simulated brain volumes of various types of MRI scans, namely T1-weighted, T2-weighted and PD-weighted. The simulated brain volumes have been obtained from BrainWeb (Collins et al., 1998), which is a freely available online database. These simulated brain volumes have been generated using an MRI simulator (Kwan et al., 1996). The thickness of slices in all brain MRI volumes is 1 mm, and the dimensions are $181 \times 217 \times 181$, in x-, y- and z-axis, respectively. Prior to several denoising experiments, which are presented in subsequent sections, we extracted the brain tissues from MRI of complete head so that the reported denoising results are not influenced by nonbrain tissues like fat and skull. The quantitative measures for different experiments have been reported by averaging the results over individual slices. To check the robustness of the proposed algorithm to noise, brain MRIs are corrupted by Rician noise of various intensities. Figure 3 shows a brain MRI slice in T1-weighted, T2-weighted and PD-weighted modalities, corrupted by different levels of Rician noise, that is, $\sigma = 7.5$, 15, 22.5, and 30, where σ represents the standard deviation of noise in the image.

The denoising step in a medical imaging workflow is critical particularly when the pathological structures are small in size. In this context, we have performed experiments on T2-weighted brain MRIs containing multiple sclerosis (MS) lesions. The T2-weighted images with MS lesions used in this work are also part of a brain volume in the BrainWeb database. These images are corrupted with Rician noise and filtered using the proposed algorithm to show its capability to preserve small pathological structures.

III. RESULTS AND DISCUSSION

In this section, the proposed algorithm has been validated on simulated T1-weighted, T2-weighted, and PD-weighted brain MRI by performing different experiments. To start with, the selection of optimal parameters' values has been described for different variants of XNLM. Then, these variants have been compared with the standard

Table II. Quantitative performance comparison of IANLM and ENLM with different variants of the proposed algorithm in terms of PSNR.

Noise (σ)	IANLM	ENLM	$XNLM_0$	$XNLM_1$	XNLM
			T1-weighted brain MRI		
7.5	32.47	36.27	36.35	36.37	**36.67**
15	26.94	31.84	32.05	32.17	**32.57**
22.5	23.58	28.89	28.75	29.25	**29.64**
30	21.15	26.83	26.29	27.17	**27.42**
			T2-weighted brain MRI		
7.5	31.68	34.76	35.70	35.72	**35.95**
15	26.61	30.19	30.85	30.94	**31.28**
22.5	23.46	27.71	27.95	28.10	**28.42**
30	21.09	25.62	25.60	25.77	**26.07**
			PD-weighted brain MRI		
7.5	32.34	36.70	37.66	37.69	**37.69**
15	27.08	31.76	32.54	32.79	**33.20**
22.5	23.83	29.34	29.48	29.98	**30.31**
30	21.45	27.47	27.40	27.89	**28.15**

IANLM and ENLM algorithm in terms of denoising and computational performance measures. Additionally, the denoising performance of the proposed algorithm has been compared with four other state of the art denoising methods. Further, the proposed algorithm has been applied to filter noisy brain MRIs with MS lesions to show the validity of the proposed algorithm in a practical pathological context. Finally, the 3D brain volume filtered by the proposed algorithm (reconstructed from corresponding 2D filtered slices) has been shown to visualize the restored structures more comprehensively.

The results of different denoising algorithms have been presented visually and quantitatively. PSNR has been used as a quantitative measure to assess the denoising performance. It measures the perceptible similarity between two images, and is computed using the following equation.

$$\mathrm{PSNR} = 10\log_{10}(R^2/\mathrm{MSE}) = 20\log_{10}(R/\mathrm{RMSE}) \tag{7}$$

where, R represents the maximum possible intensity value of a pixel in the image. For eight-bit gray level images, R is set to 255. RMSE is the root mean square error between the restored and original (ground truth) image.

The experiments in this work have been conducted on a Core i7 system with 16 GB RAM and 3.4 GHz Turbo Boost CPU. MATLAB R2013a (8.1.0.604, http://www.mathworks.com/products/matlab/) has been used as the computational tool (2011).

A. Selection of Parameters. In this section, the selection of optimal values of XNLM parameters has been discussed for brain MRI denoising. These parameters' values have been obtained after empirically testing the performance over a suitable range of their values. Moreover, the choice of optimal values is made by considering the performance at various noise levels. Table I lists the optimal values of different parameters of XNLM. In general, the parameters are applicable to all types of investigated MRI sequences, unless otherwise specified.

B. Performance Analysis of the Proposed Algorithm. In this section, the performance of different variants of the proposed XNLM algorithm has been validated on T1-weighted, T2-weighted, and PD-weighted brain MRI data. The brain MRIs have been corrupted with Rician noise of various levels, and denoising results of different variants of XNLM have been presented in terms of PSNR. The results have been compared with the basic IANLM and ENLM algorithms, and presented in Table II. The results highlighted in bold text in Table II correspond to best performance. The parameter values of IANLM and ENLM have been adopted from their respective papers (Iftikhar et al., 2013) and (Iftikhar et al., 2014). It can be immediately concluded from the results in Table II that different variants of XNLM yield considerably improved denoising results compared to IANLM and ENLM. Further, the spiral implementation of XNLM results in improved denoising performance compared to conventional row/column wise implementation, especially for higher noise levels (compare $XNLM_0$ and $XNLM_1$). It also becomes evident from Table II that the WCM procedure improves the quality of restored image (compare $XNLM_1$ and XNLM). The variants XNLM and $XNLM_2$ (implementing the proposed pixel preselection method) yield almost similar results. Therefore, the results are only presented for XNLM in Table II. The main advantage of $XNLM_2$ is to improve the computational efficiency of the algorithm, which can be verified by computational results in Section III.C. The variant XNLM, which encompasses all the proposed extensions to IANLM, consistently produces highest PSNR values in all cases. Therefore, throughout the rest of the text, the term "proposed algorithm" refers to this particular variant only.

C. Computational Performance of the Proposed Algorithm. In this section, we have compared the computational performance of XNLM with the standard IANLM algorithm. To show the computational advantage of our proposed pixel preselection procedure, we have also measured the computational performance of $XNLM_2$. The computational performance has been measured in terms of average time (number of seconds) that the algorithm consumes while denoising an input image.

Table III presents average computational results over T1-weighted, T2-weighted, and PD-weighted brain MRIs using different algorithms. The results highlighted in bold text in Table III correspond to minimum (best) computational time. It can be seen from Table III that for all noise levels that we have tested, XNLM consumes much less time to denoise images compared to $XNLM_2$ for

Table III. Computational efficiency (average time in seconds) of IANLM and different variants of the proposed algorithm.

	Average Time in Seconds								
	T1-Weighted Brain MRI			T2-Weighted Brain MRI			PD-Weighted Brain MRI		
Noise(σ)	IANLM	$XNLM_2$	XNLM	IANLM	$XNLM_2$	XNLM	IANLM	$XNLM_2$	XNLM
7.5	9.21	11.85	**6.84**	9.20	11.51	**6.44**	8.83	11.45	**7.02**
15	8.03	10.70	**7.99**	8.29	10.68	**7.30**	8.51	9.61	**7.68**
22.5	**7.54**	9.30	8.36	7.73	10.10	**7.69**	8.02	8.90	**7.99**
30	**6.39**	8.73	8.59	**7.38**	9.91	8.08	**7.76**	8.70	8.22

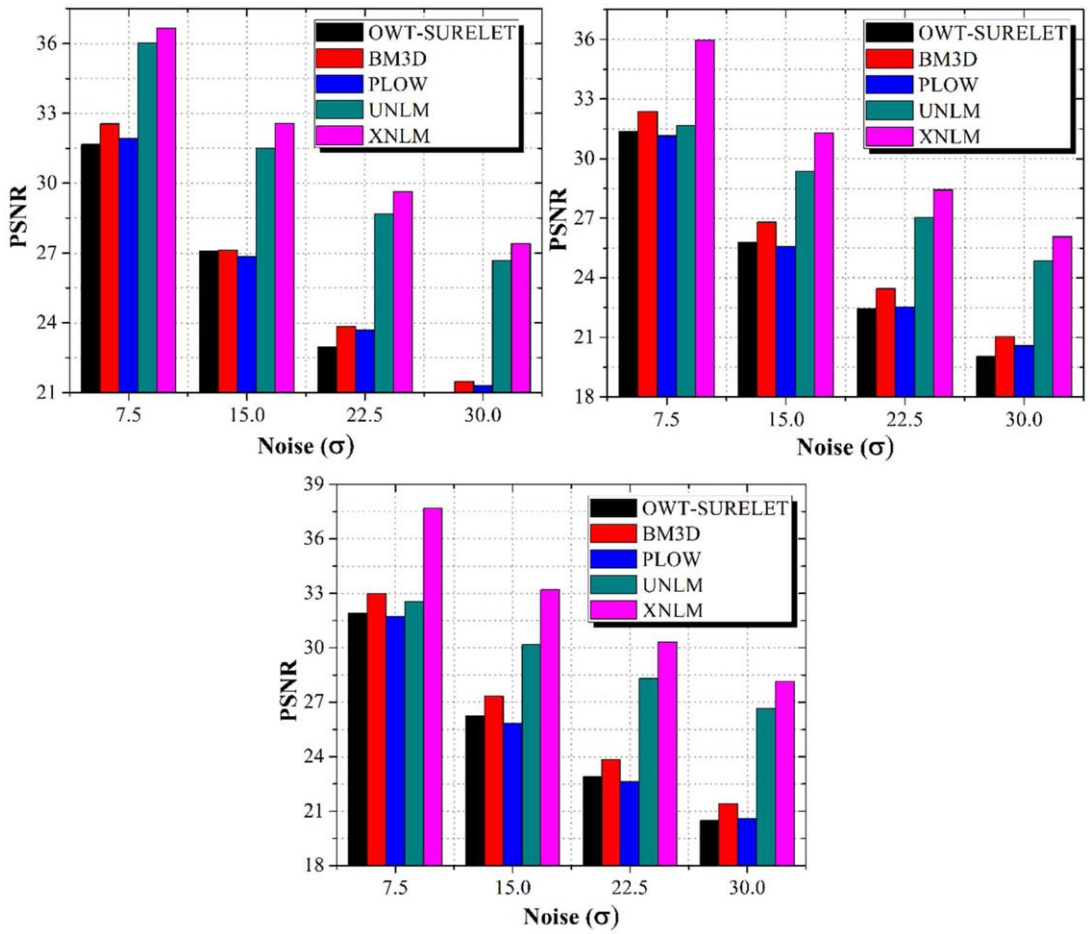

Figure 4. Performance comparison (in terms of PSNR) of XNLM with contemporary methods. (a) T1-weighted images, (b) T2-weighted images, and (c) PD-weighted images. [Color figure can be viewed in the online issue, which is available at wileyonlinelibrary.com.]

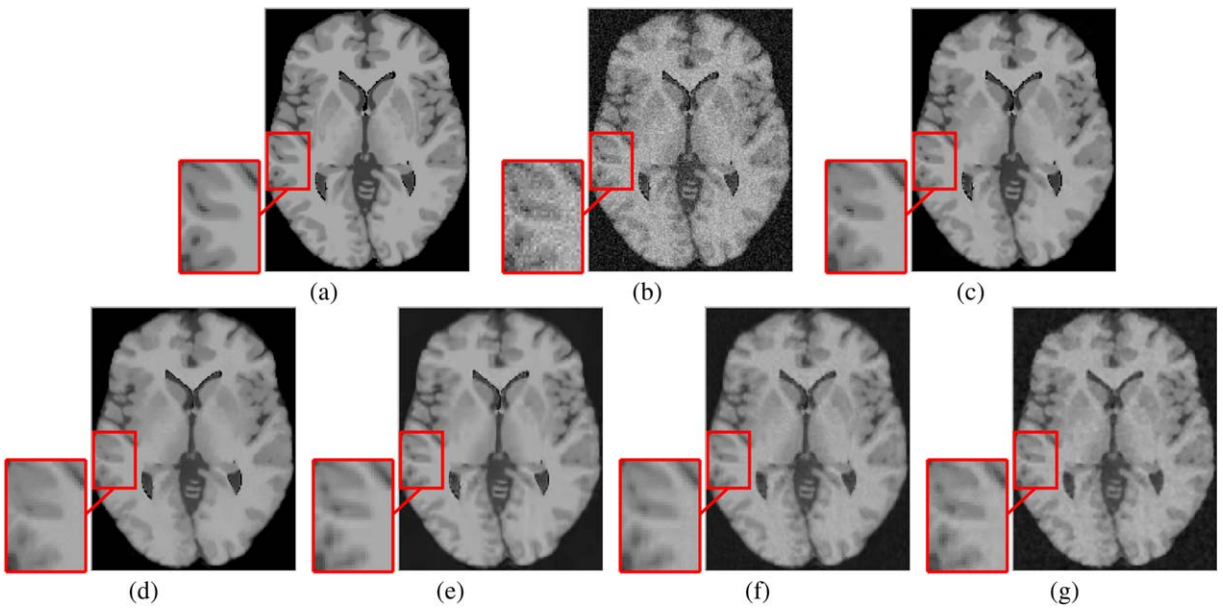

Figure 5. Visual results of filtering a noisy T1-weighted brain image. (a) Noise-free image, (b) Noisy ($\sigma = 15$) image. Images filtered by (c) XNLM (proposed), (d) UNLM, (e) BM3D, (f) PLOW, and (g) OWT-SURELET. [Color figure can be viewed in the online issue, which is available at wileyonlinelibrary.com.]

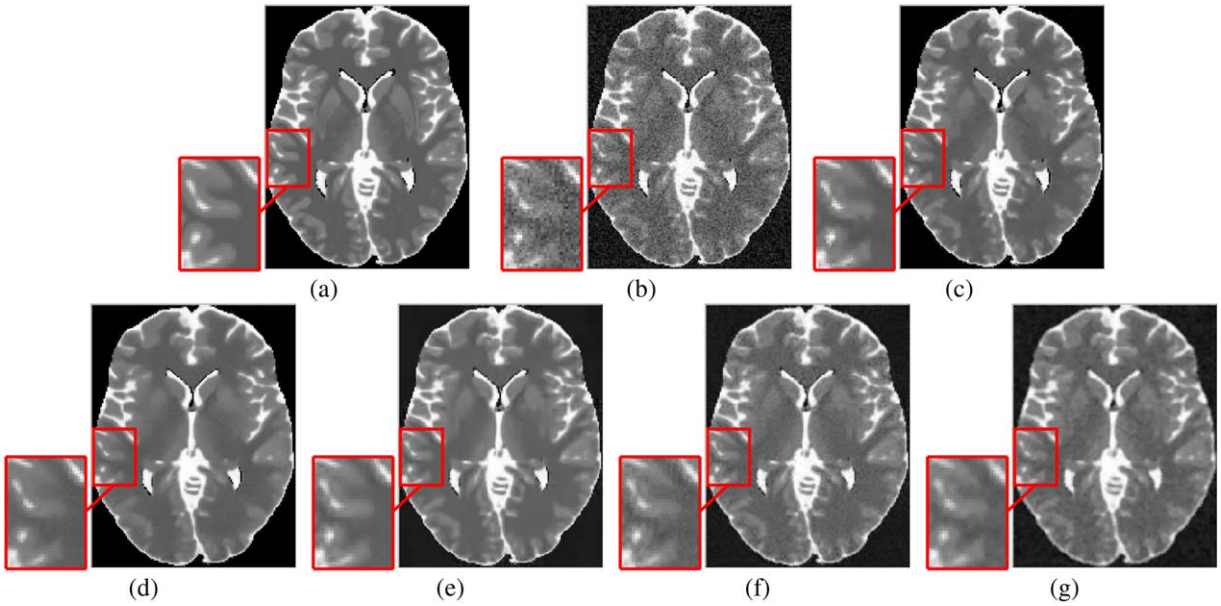

Figure 6. Visual results of filtering a noisy T2-weighted brain image. (a) Noise-free image, (b) Noisy ($\sigma = 15$) image. Images filtered by (c) XNLM (proposed), (d) UNLM, (e) BM3D, (f) PLOW, and (g) OWT-SURELET. [Color figure can be viewed in the online issue, which is available at wileyonlinelibrary.com.]

different types of MRI scans. This shows that the proposed pixel preselection process considerably reduces the computational burden of the proposed algorithm. It can also be noted that XNLM yields computational performance comparable to the original IANLM algorithm. For some noise levels, the algorithm is computationally even more efficient than IANLM. The slightly lower computational performance of the proposed XNLM algorithm can be justified by its large denoising performance advantage over IANLM. Therefore, it can be concluded that the proposed XNLM algorithm substantially increases the denoising performance without considerably suffering from computational perspective.

D. Performance Comparison with Existing Methods. To obtain a reliable assessment of the robustness of the proposed algorithm, it should be compared with state of the art denoising methods. Therefore, in this section, we have analyzed the performance of the proposed algorithm in comparison with a few popular contemporary denoising methods, namely UNLM (Manjon et al., 2008), PLOW filtering (Chatterjee and Milanfar, 2012), BM3D filtering (Dabov et al., 2007), and OWT-SURELET (Luisier et al., 2007). These methods have been already described in Section I.

The proposed XNLM algorithm and the said denoising methods have been applied to T1-weighted, T2-weighted, and PD-

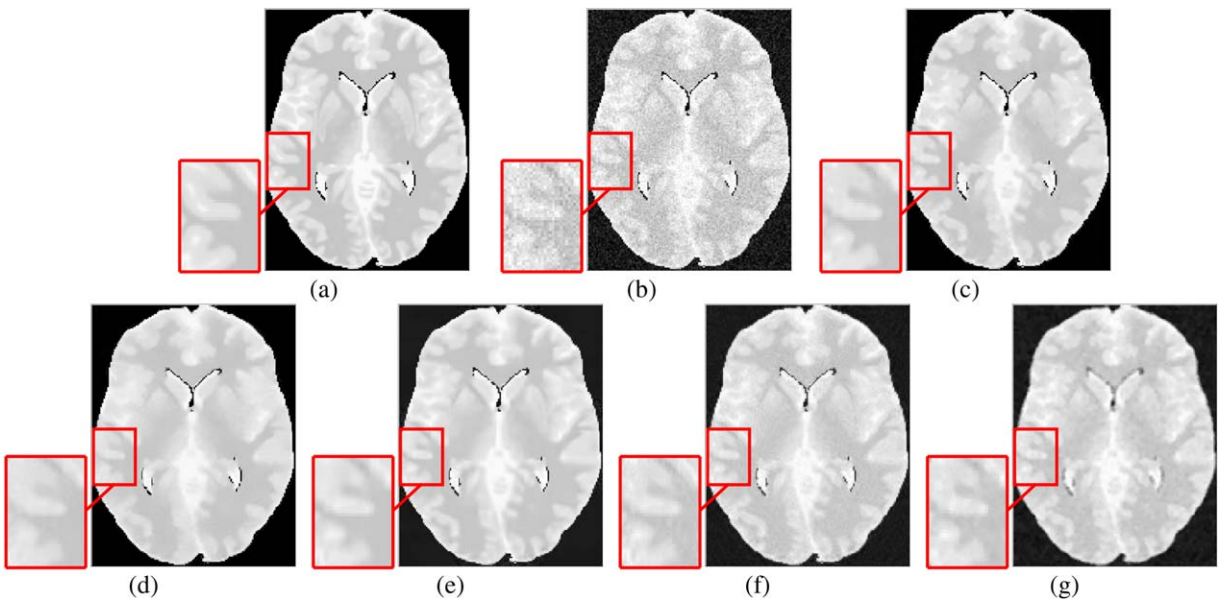

Figure 7. Visual results of filtering a noisy PD-weighted brain image. (a) Noise-free image, (b) Noisy ($\sigma = 15$) image. Images filtered by (c) XNLM (proposed), (d) UNLM, (e) BM3D, (f) PLOW, and (g) OWT-SURELET. [Color figure can be viewed in the online issue, which is available at wileyonlinelibrary.com.]

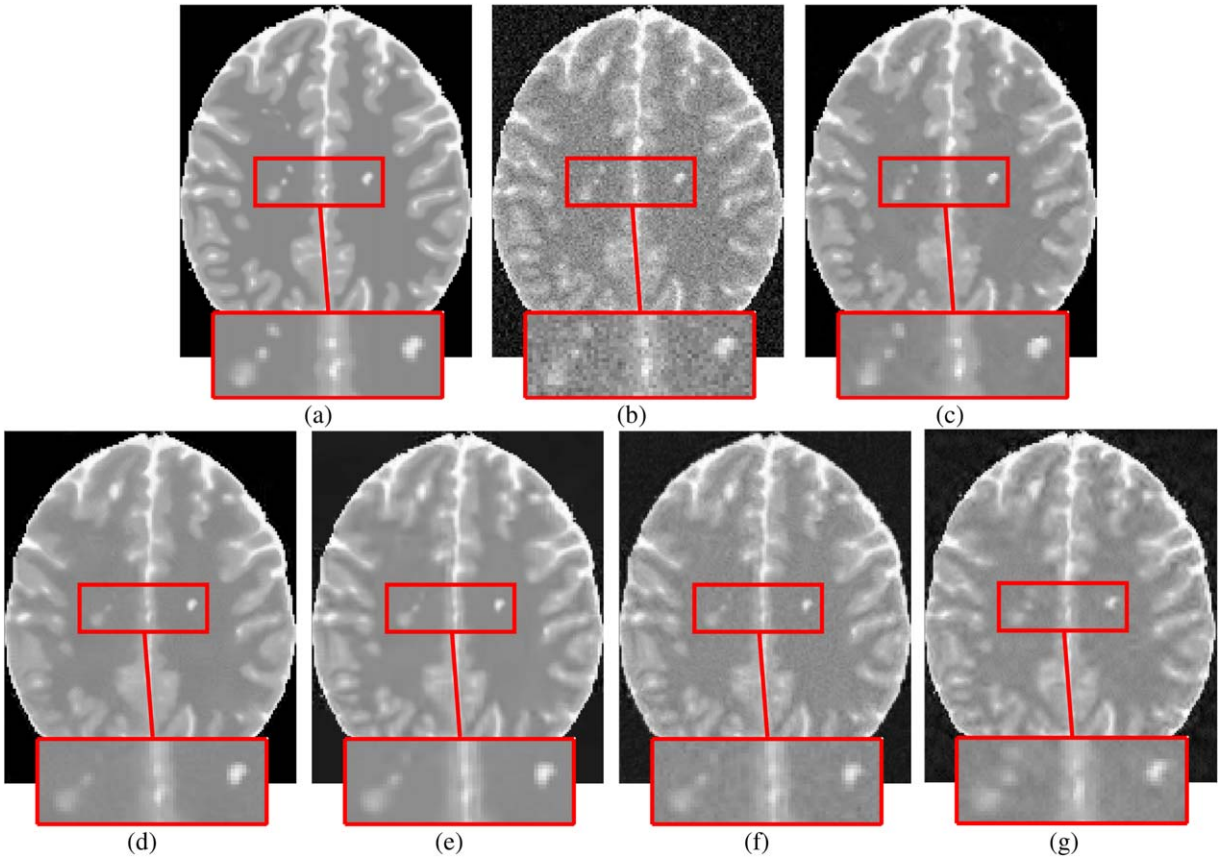

Figure 8. Visual results of denoising T2-weighted image containing MS lesion. (a) Noise-free image, (b) Noisy ($\sigma = 15$) image. Image filtered by (c) XNLM (proposed)—PSNR: 32.14, (d) UNLM—PSNR: 30.41, (e) BM3D—PSNR: 27.26, and (f) PLOW—PSNR: 26.03, (g) OWT-SURELET—PSNR: 26.46. [Color figure can be viewed in the online issue, which is available at wileyonlinelibrary.com.]

weighted brain MRIs corrupted by Rician noise of various intensities. The quantitative results in terms of PSNR have been shown graphically in Figure 4. It can be immediately noted from the Figure 4 that XNLM considerably outperforms other denoising methods. All the contemporary denoising methods lack enough robustness to noise. UNLM is the only exception, which yields somewhat comparable performance to XNLM for T1-weighted images. However, for T2-weighted and PD-weighted images, the performance of UNLM also deteriorates severely compared to XNLM. Therefore, it can be concluded that for different scan types of MRIs, the proposed algorithm is robust to noise and restores higher quality images compared to other state of the art denoising algorithms.

Figures 5–7 present visual results of denoising a particular slice from the T1-weighted, T2-weighted, and PD-weighted brain MRI volumes, respectively, using XNLM and other contemporary algorithms. For each type of MRI scan, original, noisy ($\sigma = 15$) and filtered images have been shown. In each case, the quality of the image filtered by XNLM is better compared to other denoising methods. A particular portion of each image is zoomed to show different tissues more prominently. An instant observation of the zoomed portion reveals the capability of the proposed algorithm to preserve edges and small image details. All the contemporary methods either remove the edge information by blurring the image or do not remove the potential noisy artifacts. Hence, based on quantitative and qualitative assessment, it can be concluded that the proposed algorithm is a better choice than other algorithms.

E. Preservation of Clinical Features. In this section, we have validated the proposed XNLM algorithm on a simulated noisy T2-weighted brain MRI volume with MS lesions. MS is an inflammatory disease in which the insulating covers of nerve cells in the brain are damaged. The lesions of MS are generally found in white matter (WM) of the brain and can be visualized using MRI. The performance of a CAD system using such images heavily depends on the robustness of the denoising algorithm, as the high quality of denoised images results in better segmentation, which in turn results in better classification (diagnosis) of the disease (Hassan et al., 2014). Therefore, an effective denoising algorithm prior to actual diagnosis is central to accurate analysis.

In this section, a T2-weighted brain MRI volume with MS lesions has been corrupted with Rician noise of certain level ($\sigma = 15$), and has been denoised using the proposed XNLM algorithm. The emphasis in this section is on exploring the ability of XNLM to preserve pathological information contained in MS lesions. State of the art denoising methods, used in Section III.D, have also been tested on the said brain volume. Figure 8 qualitatively compares the visual denoising results of various algorithms for a particular slice of the 3D brain MRI volume.

Visual inspection of the zoomed portion of restored images reveals that the image restored by XNLM retains the underlying

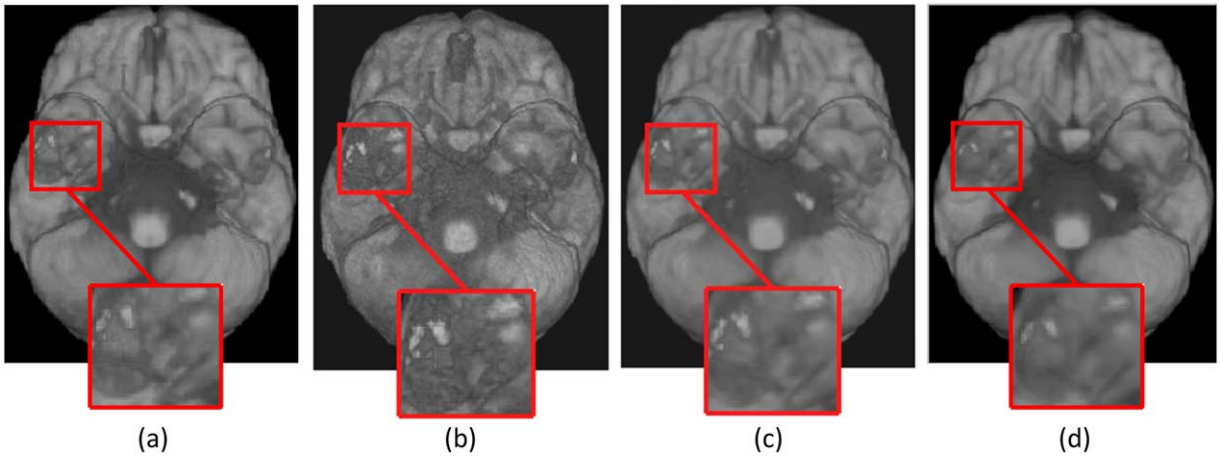

Figure 9. Visualization of 3D brain volume after reconstruction from individual slices. (a) Noise-free brain volume, (b) Noisy (σ = 15) brain volume. Brain volume reconstructed after filtering by (c) XNLM (proposed) and (d) UNLM. [Color figure can be viewed in the online issue, which is available at wileyonlinelibrary.com.]

structure/detail of the MS-lesion in the original image. On the contrary, other algorithms have either eliminated important information relevant to MS-lesion due to blurring (see Figs. 8d and 8e), or have introduced undesirable artifacts (see Figs. 8f and 8g) in the image. This phenomenon expresses the inherent capability of XNLM to retain pathologically important information, which is useful in many practical applications related to medical analysis and diagnosis. It should be noted that we have validated the proposed algorithm on all slices of the T2-weighted volume with MS lesions, however, for demonstration, results have been presented here for one slice only.

F. Visualization of Reconstructed Brain Volume. The visualization of brain volume in 3D has importance in various medical applications such as computer-aided surgery (Nakajima et al., 1997; Rieder et al., 2008). The neurologist can view the texture and orientation of different brain structures more comprehensively in 3D compared to 2D slices of a particular portion of brain. In this section, we have reconstructed the 3D brain volume from 2D slices using the MIPAV tool (McAuliffe et al., 2001). MIPAV is specially designed by Center for Information Technology at National Institutes of Health for medical image processing, analysis and visualization. For validating XNLM, we have presented the reconstructed T1-weighted brain volumes in Figure 9. The orientation of the view is from bottom of the subject head. First two columns in Figure 9 show the reconstructed simulated and noisy (σ=15) brain volumes, respectively. Whereas, last two columns show the brain volumes reconstructed after denoising the individual brain slices by XNLM and UNLM, respectively. For simplicity of presentation, results have been compared here with UNLM only, owing to its best performance among various contemporary algorithms used in Section III.D. It can be observed from Figure 9 that the proposed XNLM algorithm produces a brain volume very similar to the noise-free brain volume. The brain volume reconstructed after denoising by UNLM, conversely, has lost important structural details. This can be seen more vividly by comparing the highlighted portion of different brain volumes. Hence, the proposed XNLM algorithm is expected to perform reasonably well in medical applications, which are based on processing and visualization of 3D brain volumes.

IV. EXPERIMENTS ON REAL BRAIN MRI

In this section, we have performed experiments on real (clinical) brain MRI to investigate the practical effectiveness of the proposed XNLM algorithm. For this purpose, a T2-weighted knee MRI has been denoised using the proposed algorithm. As the amount of noise in clinical MRIs is not known in advance, some noise estimation method should be used to assess the amount of noise in clinical images. A simple, yet fairly accurate, method is to estimate the noise from the background part of square magnitude MRI (Fernandez

Figure 10. Denoising of a clinical MR image using the proposed XNLM algorithm. (a) Clinical knee MR image along with inherent noise, (b) Image filtered using XNLM, and (c) Residual image. [Color figure can be viewed in the online issue, which is available at wileyonlinelibrary.com.]

et al., 2008). According to this method, the standard deviation of noise can be estimated using the following mathematical expression.

$$\hat{\sigma} = \sqrt{\frac{1}{2N}\sum_{k=1}^{N} M_k^2} \tag{8}$$

where M_k represents the background part of the magnitude MRI, N is the number of pixels in M_k, and $\hat{\sigma}$ is the estimated standard deviation of Rician noise. The background part of the image can be obtained by any suitable threshold selection method.

Figure 10 shows a clinical MRI of knee containing inherent Rician noise, which was estimated using Eq. (8) prior to denoising using the proposed XNLM algorithm. It can be observed from Figure 10(b) that XNLM effectively removes noise from the knee image while preserving fine image details. As highlighted in Figures 10(a) and 10(b), small image structures are preserved in the filtered image. Such small structures may indicate cracks in knee, and therefore, are critical for further computer-aided analysis. Figure 10(c) also shows corresponding residual image, which is obtained by subtracting the filtered image from noisy version of the image. It is usually computed as a qualitative measure of quality of the filtered image. For adequate denoising, the residual image should contain minimal image structures (Buades et al., 2005). This can be verified from the residual image shown in Figure 10(c), which is highly uncorrelated and shows very few image structures. Thus, the proposed XNLM algorithm can be reliably used in practical medical applications.

V. CONCLUSION

An XNLM denoising algorithm has been proposed by adapting IANLM (a variant of classical NLM algorithm) to Rician noise in MRIs, and introducing a WCM procedure. The computational burden of XNLM has been reduced by proposing a parameter-free pixel preselection process, which automatically adapts to the amount of noise in the image. Different variants of XNLM have been proposed to investigate the impact of different extensions introduced in the proposed algorithm. To validate these variants, extensive experimentation has been performed on brain MRIs acquired with different types of MRI scans, namely T1-weighted, T2-weighted, and PD-weighted MRIs. These images have been corrupted by Rician noise of various levels, and the performance of the proposed variants of XNLM has been compared with standard IANLM and ENLM algorithms. Moreover, the proposed XNLM algorithm, incorporating all the introduced extensions, has been compared with a few state of the art denoising algorithms. Improved quantitative measures and qualitative results (for 2D and reconstructed 3D images) show the robustness of the proposed algorithm over other contemporary algorithms. Additionally, the proposed algorithm has been shown to preserve pathologically important information by validating it on T2-weighted brain MRI containing lesions of MS. Therefore, it can be concluded that the proposed XNLM algorithm improves the quality of results in practical medical systems.

ACKNOWLEDGMENT

The authors would also like to express our appreciation for McConnell Brain Imaging Center (BIC) of the Montreal Neurological Institute, for publicly sharing the simulated brain MR data (BrainWeb, http://www.bic.mni.mcgill.ca/brain-web). Finally, the authors are obliged to David Fernandez-Prim for providing the MATLAB on-figure magnifier tool (http://www.mathworks.com/matlabcentral/fileexchange/26007-on-figure-magnifier), which greatly simplified the presentation of figures used in this work. We would like to acknowledge Pattern Recognition Lab, DCIS, PIEAS, for providing a cooperative research environment, and its members for their continuous support in every possible way.

REFERENCES

M. Aksam, S. Rathore, and A. jalil, Parameter optimization for non-local de-noising using elite ga, IEEE 15th International Multitopic Conference (INMIC), Islamabad, 2012, pp. 194–199.

A. Buades, B. Coll, and J.M. Morel, A review of image denoising algorithms with a new one, Multiscale Model Simul 4 (2005), 490–530.

S.G. Chang, B. Yu, and M. Vetterli, Adaptive wavelet thresholding for image denoising and compression, IEEE Trans Image Process 9 (2000), 1532–1546.

P. Chatterjee and P. Milanfar, Patch-based near-optimal image denoising, IEEE Trans Image Process 21 (2012), 1635–1649.

D.L. Collins, A.P. Zijdenbos, V. Kollokian, J.G. Sled, N.J. Kabani, C.J. Holmes, and A.C. Evans, Design and construction of a realistic digital brain phantom, IEEE Trans Med Imaging 17 (1998), 463–468.

P. Coupe, P. Hellier, S. Prima, C. Kervrann, and C. Barillot, 3d wavelet subbands mixing for image denoising, Int J Biomed Imaging 2008 (2008), 1–11.

P. Coupe, P. Yger, S. Prima, P. Hellier, C. Kervrann, and C. Barillot, An optimized blockwise nonlocal means denoising filter for 3-d magnetic resonance images, IEEE Trans Med Imaging 27 (2008), 425–441.

K. Dabov, A. Foi, V. Katkovnik, and K.O. Egiazarian, Image denoising by sparse 3-d transform-domain collaborative filtering, IEEE Trans Image Process 16 (2007), 2080–2095.

D. Donoho, De-noising by soft-thresholding, IEEE Trans Inf Theory 41 (1995), 613–627.

D.L. Donoho and I.M. Johnstone, Minimax estimation via wavelet shrinkage, Ann Stat 26 (1998), 879–921.

S.A. Fernandez, C.A. Lopez, and C.F. Westin, Noise and signal estimation in magnitude mri and rician distributed images: A lmmse approach, IEEE Trans Image Process 17 (2008), 1383–1398.

I.K. Fodor and C. Kamath, Denoising through wavelet shrinkage: An empirical study, J Electron Imaging 12 (2003), 151–160.

G. Gilboa, N. Sochen, and Y.Y. Zeevi, Image enhancement and denoising by complex diffusion processes, IEEE Trans Pattern Anal Mach Intell 26 (2004), 1020–1036.

D. Gupta, R.S. Anand, and B. Tyagi, Edge preserved enhancement of medical images using adaptive fusion–based denoising by shearlet transform and total variation algorithm, J Electron Imaging 22 (2013), 043016.

M. Hassan, A. Chaudhry, A. Khan, and M.A. Iftikhar, Robust information gain based fuzzy c-means clustering and classification of carotid artery ultrasound images, Comput Methods Programs Biomed 113 (2014), 593–609.

M.A. Iftikhar, A. Jalil, S. Rathore, A. Ali, and M. Hussain, Brain MRI denoizing and segmentation based improved adaptive non-local means, Int J Imaging Syst Technol 23 (2013), 235–248.

M.A. Iftikhar, A. Jalil, S. Rathore, and M. Hussain, Robust brain mri denoising and segmentation using enhanced non-local means algorithm, Int J Imaging Syst Technol 24 (2014), 52–66.

R.K.S. Kwan, A.C. Evans, and G.B. Pike, "An extensible mri simulator for post-processing evaluation," In Visualization in biomedical computing, K.H. Höhne and R. Kikinis (Editors), Vol. 1131, Springer-Verlag, Hamburg, Germany, 1996, pp. 135–140.

F. Luisier, T. Blu, and M. Unser, A new sure approach to image denoising: Interscale orthonormal wavelet thresholding, IEEE Trans Image Process 16 (2007), 593–606.

J.V. Manjon, J.C. Caballero, J.J. Lull, G.G. Marti, L.M. Bonmati, and M. Robles, Mri denoising using non-local means, Med Image Anal 12 (2008), 514–523.

J.V. Manjon, P. Coupe, L.M. Bonmatí, D.L. Collins, and M. Robles, Adaptive non-local means denoising of mr images with spatially varying noise levels, J Magn Reson Imaging 31 (2010), 192–203.

M.J. McAuliffe, F.M. Lalonde, D. McGarry, W. Gandler, K. Csaky, and B.L. Trus, Medical image processing, analysis & visualization in clinical research, 14th Symposium on IEEE Computer-Based Medical Systems, Bethesda, MD, 2001, pp. 381–386.

S. Nakajima, H. Atsumi, A. Bhalerao, F. Jolesz, R. Kikinis, T. Yoshimine, T. Moriarty, and P. Stieg, Computer-assisted surgical planning for cerebrovascular neurosurgery, Neurosurgery 41 (1997), 403–410.

W.-D. Nicolas, S. Prima, P. Coupé, S.P. Morrissey, and C. Barillot, Rician noise removal by non-local means filtering for low signal-to-noise ratio mri: Applications to DT-MRI, Med Image Comput Comput Assist Interv 11 (2008), 171–179.

R.D. Nowak, Wavelet-based rician noise removal for magnetic resonance imaging, IEEE Trans Image Process 8 (1999), 1408–1419.

R.e. Öktem, L. Yaroslavsky, K. Egiazarian, and J. Astola, Transform domain approaches for image denoising, J Electron Imaging 11 (2002), 149–156.

S. Osher, M. Burger, D. Goldfarb, J. Xu, and W. Yin, An iterative regularization method for total variation-based image restoration, Multiscale Model Simul 4 (2005), 460–489.

P. Perona and J. Malik, Scale-space and edge detection using anisotropic diffusion, IEEE Trans Pattern Anal Mach Intell 12 (1990), 629–639.

C. Rieder, F. Ritter, M. Raspe, and H.-O. Peitgen, Interactive visualization of multimodal volume data for neurosurgical tumor treatment, Comput Graph Forum 27 (2008), 1055–1062.

I.W. Selesnick, The double-density dual-tree dwt, IEEE Trans Signal Process 52 (2004), 1304–1314.

L. Szilagyi, Z. Benyo, S.M. Szilagyi, and H.S. Adam, Mr brain image segmentation using an enhanced fuzzy c-means algorithm, Proceedings of the 25th Annual International Conference of Engineering in Medicine and Biology Society, Cancun, Mexico, Vol. 721, 2003, pp. 724–726.

C. Tomasi and R. Manduchi, Bilateral filtering for gray and color images, Sixth International Conference on Computer Vision, Bombay, India, 1998, pp. 839–846.

The MathWorks Incorporation, Matlab—the language of technical computing, The MathWorks Incorporation, Natick, Massachusetts, 2011.

A.T. Vega, V.G. Perez, S.A. Fernandez, and C.F. Westin, Efficient and robust nonlocal means denoising of mr data based on salient features matching, Comput Methods Programs Biomed 105 (2012), 131–144.

J. Wen, Y. Li, and W. Wang, Wavelet-based denoising and its impact on analytical spect reconstruction with nonuniform attenuation compensation, Int J Imaging Syst Technol 23 (2013), 36–43.